ATLAS NOTE

ATLAS-CONF-2016-075

3rd August 2016

Search for supersymmetry in events with four or more leptons in $\sqrt{s} = 13$ TeV pp collisions using 13.3 fb^{-1} of ATLAS data.

The ATLAS Collaboration

ATLAS-CONF-2016-075
08 August 2016

Abstract

Results from a search for supersymmetry in events with four or more leptons (electrons and muons) are presented. The analysis uses a data sample corresponding to 13.3 fb^{-1} of proton–proton collisions delivered by the Large Hadron Collider at $\sqrt{s} = 13$ TeV and recorded by the ATLAS detector. No significant deviations from Standard Model predictions are observed in data and results are used to set upper limits on the event yields from processes beyond the Standard Model. Exclusion limits are set at the 95% confidence level in a simplified model of chargino production with indirect RPV decays.

1 Introduction

Supersymmetry (SUSY) [1–6] is a space-time symmetry that postulates the existence of new particles with spin differing by one half-unit with respect to their Standard Model (SM) partners. In supersymmetric extensions of the SM, each SM fermion (boson) is associated with a SUSY boson (fermion), having the same quantum numbers as its partner except for spin. The introduction of these new SUSY particles provides a potential solution to the hierarchy problem [7–10].

The charginos and neutralinos are mixtures of the bino, winos and higgsinos, which are superpartners of the U(1) and SU(2) gauge bosons, and the Higgs bosons, respectively. Their mass eigenstates are referred to as charginos $\tilde{\chi}_i^{\pm}$ ($i = 1, 2$) and neutralinos $\tilde{\chi}_j^0$ ($j = 1, 2, 3, 4$), in order of increasing mass. The direct production of charginos and neutralinos could be the most abundant mode of SUSY production at the Large Hadron Collider (LHC) if the masses of the gluinos and squarks are large.

In generic SUSY models with minimal particle content, the superpotential includes terms that violate conservation of lepton (L) and baryon (B) number [11, 12]:

$$\frac{1}{2}\lambda_{ijk}L_iL_j\bar{E}_k + \lambda'_{ijk}L_iQ_j\bar{D}_k + \frac{1}{2}\lambda''_{ijk}\bar{U}_i\bar{D}_j\bar{D}_k + \kappa_iL_iH_2, \tag{1}$$

where L_i and Q_i indicate the lepton and quark SU(2)-doublet superfields, respectively, and $\bar{E}_i$, $\bar{U}_i$ and $\bar{D}_i$ are the corresponding singlet superfields. Quark and lepton generations are referred to by the indices i, j and k, while the Higgs field that couples to up-type quarks is represented by the Higgs SU(2)-doublet superfield H_2. The λ_{ijk}, λ'_{ijk} and λ''_{ijk} parameters are nine new Yukawa couplings satisfying $\lambda_{jik} = -\lambda_{ijk}$, while the κ_i parameters have dimensions of mass and vanish at the unification scale.

In the absence of a protective symmetry, L- and B-violating terms could allow for proton decay at a rate that is in conflict with the tight experimental constraints on the proton lifetime [13]. This conflict can be avoided by imposing the conservation of R-parity [14], defined as $(-1)^{3(B-L)+2S}$, where S is spin, or by explicitly conserving either B or L in the Lagrangian in R-parity-violating (RPV) scenarios. In RPV models, the lightest SUSY particle (LSP) is unstable and decays to SM particles, including charged leptons and neutrinos when at least one of the λ_{ijk} parameters (violating L, but not B) is non-zero. RPV SUSY scenarios can therefore result in signatures with high lepton multiplicities and substantial missing transverse momentum, selections on which can be used to suppress SM background processes effectively.

A search is presented for new physics in final states with at least four isolated leptons (electrons and muons). A total of 13.3 fb^{-1} of proton-proton collision data delivered by the LHC at 13 TeV in 2015 and 2016 are analysed. The search itself is model-independent, and results are presented in terms of the visible cross-section for new physics processes with this signature. The results are also interpreted in terms of a SUSY model of chargino production with indirect RPV decays, where the chargino decay to the LSP is R-parity-conserving (RPC), and the LSP undergoes an RPV decay.

This analysis closely follows the 7 TeV [15] and 8 TeV analyses [16]. Previous searches for SUSY particles using signatures with three or more leptons have been carried out at the Tevatron collider [17–22], and at the LHC by the ATLAS experiment [15, 16, 23–25] and the CMS experiment [26–30].

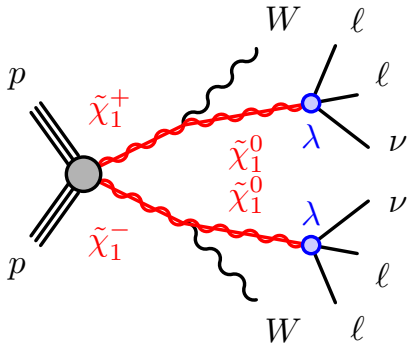

Figure 1: Diagram of the benchmark SUSY model of chargino production with indirect RPV decays.

2 SUSY scenarios

In the benchmark model considered for this analysis, wino-like charginos are pair-produced, and the LSP is a bino-like neutralino. The $\tilde{\chi}_1^\pm$ decays to the LSP while emitting a W boson, as shown in Figure 1. The subsequent $\tilde{\chi}_1^0$ decay is mediated by the $\frac{1}{2}\lambda_{ijk}L_iL_j\bar{E}_k$ term in Eq. 1, allowing each LSP to undergo a lepton-number-violating RPV decay:

$$\tilde{\chi}_1^0 \to \ell_k^\pm \ell_{i/j}^\mp \nu_{j/i}, \tag{2}$$

with the allowed lepton flavours depending on the indices of the associated λ_{ijk} couplings. Thus, every signal event contains a minimum of four charged leptons, and potentially up to six if both W bosons decay leptonically.

In principle, the nine λ_{ijk} RPV couplings allow the $\tilde{\chi}_1^0$ to decay to every possible combination of charged lepton pairs. The scenarios considered here include decays to electrons and muons only, with a branching fraction of 1/3 each for $\tilde{\chi}_1^0 \to e^+e^-\nu$, $\tilde{\chi}_1^0 \to e^\pm\mu^\mp\nu$ and $\tilde{\chi}_1^0 \to \mu^+\mu^-\nu$. Terms with non-zero values of the λ_{121} and λ_{122} couplings can give rise to these $\tilde{\chi}_1^0$ decays, and in the following we refer to these SUSY scenarios as $LL\bar{E}12k$ ($k = 1, 2$). However, the $\tilde{\chi}_1^0$ branching fractions cannot be reproduced by a single non-zero $LL\bar{E}$ coupling. Instead, interpretations in "pure" coupling scenarios can be obtained by appropriate reweighting of the simulated events, analogous to the procedures used in Ref. [31].

Chargino masses of 500 – 1200 GeV are studied for the $LL\bar{E}12k$ scenarios, where the LSP masses range from 10 GeV $\leq m(\tilde{\chi}_1^0) \leq m(\tilde{\chi}_1^\pm) - 10$ GeV to ensure both the RPC cascade and the RPV LSP decay are prompt. Over this chargino mass range, the $\tilde{\chi}_1^+\tilde{\chi}_1^-$ production cross-section varies from about 22 fb to about 0.2 fb [32, 33].

3 The ATLAS detector

The ATLAS detector [34] is a multipurpose particle physics detector with forward-backward symmetric cylindrical geometry[1]. The inner tracking detector (ID) covers $|\eta| < 2.5$ and consists of a silicon pixel

[1] ATLAS uses a right-handed coordinate system with its origin at the nominal interaction point (IP) in the center of the detector and the z-axis along the beam pipe. The x-axis points from the IP to the center of the LHC ring, and the y-axis points upward. Cylindrical coordinates (r, ϕ) are used in the transverse plane, ϕ being the azimuthal angle around the z-axis. The pseudorapidity is defined in terms of the polar angle θ as $\eta = -\ln\tan(\theta/2)$. Rapidity is defined as

detector, a semiconductor microstrip detector, and a transition radiation tracker. The innermost pixel layer, the insertable B-layer [35], was added between Run 1 and Run 2 of the LHC. The ID is surrounded by a thin superconducting solenoid providing a 2 T axial magnetic field. A high-granularity lead/liquid-argon sampling calorimeter measures the energy and the position of electromagnetic showers within $|\eta| < 3.2$. Sampling calorimeters with liquid argon as the active medium are also used to measure hadronic showers in the endcap ($1.5 < |\eta| < 3.2$) and forward ($3.1 < |\eta| < 4.9$) regions, while a steel/scintillator tile calorimeter measures hadronic showers in the central region ($|\eta| < 1.7$). The muon spectrometer (MS) surrounds the calorimeters and consists of three large superconducting air-core toroid magnets, each with eight coils, a system of precision tracking chambers ($|\eta| < 2.7$), and fast trigger chambers ($|\eta| < 2.4$). A two-level trigger system [36] selects events to be recorded for offline analysis.

4 Monte Carlo simulation

Monte Carlo (MC) generators are used to simulate SM processes and new physics signals. The SM processes considered are those that can lead to signatures with four reconstructed leptons. Details of the signal and background MC simulation samples used in this note, as well as the order of cross-section calculations in perturbative QCD used for yield normalization, are shown in Table 1.

For all MC simulation samples, the propagation of particles through the ATLAS detector is modelled with GEANT 4 [37] using the full ATLAS detector simulation [38] ("Fullsim"), or a fast simulation using a parametrization of the response of the electromagnetic and hadronic calorimeters [38] and GEANT 4 elsewhere ("AF-II"). The effect of multiple proton–proton collisions in the same or nearby bunch crossings (in-time and out-of-time pileup) is incorporated into the simulation by overlaying additional minimum-bias events generated with PYTHIA 8 onto hard-scatter events. Simulated events are weighted to match the distribution of the mean number of interactions per bunch crossing in data, and are reconstructed in the same manner as data. The simulated MC samples are corrected to account for differences with respect to the data in the lepton efficiencies, and the energy and momentum measurements of leptons and jets.

5 Event selection

Events recorded during stable data-taking conditions are used in the analysis if the reconstructed primary vertex has at least two tracks with transverse momentum $p_{\mathrm{T}} > 400$ MeV associated with it. The primary vertex of an event is identified as the vertex with the highest Σp_{T}^2 of associated tracks. After the application of beam, detector and data-quality requirements, the total luminosity considered in this analysis corresponds to $13.3\,\mathrm{fb}^{-1}$.

Electron candidates are required to have $|\eta| < 2.47$ and $p_{\mathrm{T}} > 7$ GeV, where the p_{T} and η are determined from the calibrated clustered energy deposits in the electromagnetic calorimeter and the matched ID track, respectively. Electrons must satisfy "very loose" likelihood-based identification criteria, defined in Ref. [46]. Muon candidates are reconstructed by combining tracks in the ID and tracks in the MS [47], and are required to have $|\eta| < 2.7$ and $p_{\mathrm{T}} > 5$ GeV. Muons must satisfy "medium" identification requirements

$y = 0.5 \ln [(E + p_z)/(E - p_z)]$ where E denotes the energy and p_z is the component of the momentum along the beam direction.

Process	Generator(s)	Full/fast sim	Cross-section calculation	UE tune	PDF set
$t\bar{t}Z, t\bar{t}W, t\bar{t}WW$	MadGraph 5_aMC@NLO [39] + Pythia 8 [40]	Fullsim	NLO	A14	NNPDF23LO
$t\bar{t}Z^{\dagger}$	Sherpa [41]	AF-II	NLO	Default	CT10
tWZ	aMC@NLO [42] + Pythia 8	Fullsim	NLO	A14	NNPDF23LO
ZZ, WZ, WW	Powheg [43] + Pythia 8	Fullsim	NLO	AZNLO	CTEQ6L1
$ZZ^{\dagger}$	Sherpa	AF-II	NLO	Default	CT10
$t\bar{t}$	Powheg + Pythia 6 [44]	Fullsim	NNLO+NNLL	Perugia2012	CT10
Z+jets, W+jets	MadGraph 5_aMC@NLO + Pythia 8	Fullsim	NNLO	A14	NNPDF23LO
Higgs (ggF, VH, VBF H)	Powheg + Pythia 8	Fullsim	NNLO+NNLL	Perugia2012	CT10
$t\bar{t}$H	aMC@NLO + Pythia 8	Fullsim	NLO	UE EE5	CTEQ6L1 (CT10ME)
VVV	Sherpa	Fullsim	NLO	Default	CT10
$tt\bar{t}, t\bar{t}t\bar{t}$	MadGraph 5_aMC@NLO + Pythia 8	Fullsim	NLO	A14	NNPDF23LO
$b\bar{b}, c\bar{c}$	Pythia 8	Fullsim	NLO	A14	NNPDF23LO
SUSY signal	MadGraph 5 [45] + Pythia 8	AF-II	NLO	A14	NNPDF23LO

Table 1: Summary of the simulated SM background samples used in this analysis, where $V = W, Z$. Samples marked with a † are used for a cross-check of yields and systematic studies.

based on the number of hits in the different ID and MS subsystems, and the significance of the charge-to-momentum ratio, defined in Ref. [47]. Events containing one or more muons that have a transverse impact parameter with respect to the primary vertex $|d_0| > 0.2$ mm or a longitudinal impact parameter with respect to the primary vertex $|z_0| > 1$ mm are rejected to suppress the cosmic-ray muon background.

Jets are reconstructed with the anti-k_t algorithm [48] with a radius parameter of $R = 0.4$. Three-dimensional calorimeter energy clusters are used as input to the jet reconstruction, and jets are calibrated following Ref. [49]. Jets must have $|\eta| < 2.8$ and $p_{\mathrm{T}} > 20$ GeV. To reduce pile-up effects, jets with $p_{\mathrm{T}} < 60$ GeV and $|\eta| < 2.4$ must have a significant fraction of the tracks associated with each jet originating from the primary vertex [50]. Events containing jets failing to satisfy the quality criteria described in Ref. [51] are rejected to suppress events with large calorimeter noise and noncollision backgrounds.

The missing transverse momentum, $E_{\mathrm{T}}^{\mathrm{miss}}$, is the magnitude of the negative vector sum of the transverse momenta of all identified physics objects (electrons, photons, muons and jets) and an additional soft term [52]. The soft term is constructed from the tracks associated to the primary vertex, but not associated with physics objects, which allows the soft term to be nearly independent of pile-up.

To avoid potential ambiguities among physics objects, candidate leptons and jets must survive "overlap removal", applied in the following order:

1. Any electron sharing an ID track with a muon is removed.
2. Jets within $\Delta R = \sqrt{(\Delta y)^2 + (\Delta\phi)^2} = 0.2$ of an electron candidate are discarded.
3. Electrons within $\Delta R = 0.4$ of a jet candidate are discarded, to suppress electrons from semileptonic decays of c- and b-hadrons.
4. Jets with fewer than two associated tracks or with a nearby muon with a significant fraction of the jet p_{T} ($p_{\mathrm{T}}^{\mu} > 0.5 p_{\mathrm{T}}^{\mathrm{jet}}$ and $p_{\mathrm{T}}^{\mu} > 0.7 \sum p_{\mathrm{T}}^{\mathrm{jet\ tracks}}$, where p_{T}^{μ}, $p_{\mathrm{T}}^{\mathrm{jet}}$ and $p_{\mathrm{T}}^{\mathrm{jet\ tracks}}$ are the p_{T} of the muon,

jet and jet tracks, respectively) are discarded either if the candidate muon is within $\Delta R = 0.2$ or if the muon can be matched to a track associated with the jet.

5. Muons within $\Delta R = 0.4$ of a jet candidate are discarded to suppress muons from semileptonic decays of c- and b-hadrons.

Finally, to suppress low-mass decays, if surviving electrons and muons form an opposite-sign (OS) pair with $m_{\mathrm{OS}} < 4$ GeV, or form a same-flavour, opposite-sign (SFOS) pair close to the Υ resonances mass range $8.4 < m_{\mathrm{SFOS}} < 10.4$ GeV, both leptons are discarded.

"Signal" leptons are candidate leptons surviving overlap removal and matching additional identification criteria. Signal electrons and muons must pass p_{T}-dependent isolation requirements, to reduce the contributions from semileptonic decays of hadrons and jets misidentified as prompt leptons. The isolation requirements use calorimeter- and track-based information to obtain 95% efficiency for leptons with $p_{\mathrm{T}} = 25$ GeV in $Z \to e^+e^-, \mu^+\mu^-$ events, rising to 99% efficiency at $p_{\mathrm{T}} = 60$ GeV. To further suppress electrons and muons originating from secondary vertices, $|z_0 \sin\theta|$ is required to be less than 0.5 mm, and the d_0 normalized to its uncertainty is required to be small, with $|d_0|/\sigma_{d_0} < 5(3)$ for electrons (muons). Signal electrons must also satisfy "medium" likelihood-based identification criteria [46].

Events are selected using a combination (logical OR) of single lepton, dilepton and trilepton triggers, and leptons must satisfy the corresponding offline p_{T}-threshold requirements shown in Table 2. Trigger thresholds for data recorded in 2016 are in some cases higher than in 2015 due to increases in beam luminosity.

Trigger	Offline p_{T} threshold [GeV]	
	2015	2016
Single isolated e	25	25
Single non-isolated e	61	61
Single isolated μ	21	25
Single non-isolated μ	51	41 or 51
Double e	14,14	16,16
Double μ	11,11	11,11 or 15,15
	19,9	21,9
Triple e	18,10,10	18,10,10
Triple μ	19,5,5	21,5,5
	7,7,7	7,7,7
Combined $e\mu$	18(e),15(μ)	18(e),15(μ)
	25(e),9(μ)	25(e),9(μ)
	8(e),25(μ)	8(e),25(μ)
	13(e),13(e),11(μ)	13(e),13(e),11(μ)
	13(e),11(μ),11(μ)	13(e),11(μ),11(μ)

Table 2: The triggers used in the analysis in 2015 and 2016 and the offline p_{T} threshold used ensuring that the lepton(s) triggering the event are in the plateau region of the trigger efficiency. Thresholds on triggers for data recorded in 2016 are higher than in 2015 due to the increase in beam luminosity, and "or" denotes a move to a higher threshold trigger during data taking. Events are used if any of the triggers is passed. Muons are triggered within a range of $|\eta| < 2.4$.

Events with four or more signal leptons (e, μ) are selected and those consistent with containing a leptonic Z-boson decay are vetoed. This Z veto rejects events where any SFOS lepton pair combination has an invariant mass close to the Z boson mass, in the range 81.2 − 101.2 GeV. To suppress radiative Z-boson decays, the Z veto also considers combinations of any SFOS pair with an additional lepton (SFOS+ℓ), or with a second SFOS pair (SFOS+SFOS), and rejects events where either the SFOS+ℓ or the SFOS+SFOS invariant mass lies in the range 81.2 − 101.2 GeV.

The effective mass of the event, m_{eff}, is used to separate the SM background from SUSY signal, where m_{eff} is defined as the scalar sum of the $E_{\text{T}}^{\text{miss}}$, the p_{T} of signal leptons and the p_{T} of jets with $p_{\text{T}} > 40$ GeV. The $p_{\text{T}} > 40$ GeV threshold on jets aims to suppress contributions from pile-up and the underlying event. Two signal regions (SR) are defined: a general signal region (SRA) with $m_{\text{eff}} > 600$ GeV, and a tighter signal region (SRB) with $m_{\text{eff}} > 900$ GeV, optimised for the $LL\bar{E}12k$ models considered here. The signal region definitions can be seen in Table 3, along with the definitions for the control regions (CR) and validation regions (VR) discussed in Section 6.

Sample	$N(e,\mu)$ signal	$N(e,\mu)$ loose	Z boson	m_{eff} [GeV]
SRA	>= 4	>= 0	veto	> 600
CR-SRA	= 2	>= 2	veto	> 600
SRB	>= 4	>= 0	veto	> 900
CR-SRB	= 2	>= 2	veto	> 900
VR	>= 4	>= 0	veto	< 600
CR-VR	= 2	>= 2	veto	< 600

Table 3: Signal region, control region, and validation region definitions. Loose leptons are candidate leptons surviving overlap removal that do not pass signal lepton criteria.

6 Background determination

Several SM processes can result in signatures appearing like SUSY signals with four reconstructed leptons, including both "real" and "fake" lepton contributions. Here, a real lepton is a prompt and genuinely isolated lepton, while a fake lepton is a non-prompt or non-isolated lepton that could originate either from semi-leptonic decays of b and c hadrons, or from mis-identification of light flavour jets, or from photon conversions. The SM processes are classified into two categories:

Irreducible background: processes leading to events with four or more real leptons.
ZZ, $t\bar{t}Z$, $t\bar{t}WW$, tWZ, VVZ (ZZZ, WZZ, WWZ), Higgs (gluon fusion H, associated production VH, vector boson fusion H, $t\bar{t}$H), $t\bar{t}t\bar{t}$, $t\bar{t}tW$.

Reducible background: processes leading to events with at least one fake lepton. Processes listed under irreducible that do not undergo a decay to four real leptons are also included in the reducible background.

1 fake lepton: WZ, WWW, $t\bar{t}W$.

2 fake leptons: $t\bar{t}$, Z+jets.

Backgrounds with three or more fake leptons (e.g. W+jets) are found to be negligible for this analysis.

In the signal regions, the irreducible background is dominated by $t\bar{t}Z$, VVZ ($V = W, Z$), and ZZ, while the reducible background is dominated by the 2-fake lepton background $t\bar{t}$. The irreducible and 1-fake lepton backgrounds are estimated from MC simulation, while the 2-fake lepton backgrounds are measured in data with the "fake factor method". The predictions for irreducible and reducible backgrounds are tested in validation regions (Section 6.2).

In the fake factor method, the number of 2-fake lepton background events in a given region is estimated from data using MC-based probabilities for a fake lepton to pass or fail the signal lepton selection. The ratio $F = f/\bar{f}$ for fake leptons is the "fake factor", where f ($\bar{f}$) is the probability that a fake lepton is misidentified as a signal (loose) lepton. Loose leptons are candidate leptons surviving overlap removal that do not pass signal lepton criteria. A control region in data is used for the extraction of the 2-fake lepton predictions. The CR definition only differs from that of the associated SR in the quality of the required leptons; exactly two signal leptons and at least two loose leptons are required, as shown in Table 3.

Fake factors are calculated separately for light-flavour jets, heavy-flavour jets and photon conversions (electrons only). These categories are referred to as fake lepton "types". The dependence of the fake factor on the lepton p_{T} and η is taken into account; however, the small dependence of the fake factor on the hard process ($t\bar{t}$, Z+jets) is neglected, since $t\bar{t}$ dominates the 2-fake lepton background in the signal regions.

To account correctly for the relative abundances of fake lepton types and production processes, a weighted average F_w of fake factors is computed in each CR, as:

$$F_w = \sum_i \left(R^i \times F^i \right). \tag{3}$$

The factor R^i is a "process fraction" that depends on the fraction of fake leptons of type i determined from MC simulation in the control region, while F^i is the corresponding fake factor calculated using MC simulation. For each fake lepton type, the fake factor from MC simulation is assumed to describe data within 25%, and this systematic uncertainty is validated by comparing leptons from heavy flavour jets in MC simulation and data. The comparison is made in a $b\bar{b}$-dominated control sample, which selects events with only one b-tagged jet containing a muon, and an additional signal or loose lepton.

The number $N_{\mathrm{red}}^{\mathrm{SR}}$ of background events with two fake leptons from reducible sources in each SR can be determined from the number of events in data in the corresponding CR, $N_{\mathrm{data}}^{\mathrm{CR}}$, according to:

$$N_{\mathrm{red}}^{\mathrm{SR}} = [N_{\mathrm{data}}^{\mathrm{CR}} - N_{\mathrm{irr,1\text{-}fake}}^{\mathrm{CR}}] \times F_{w,1} \times F_{w,2}, \tag{4}$$

where $F_{w,1}$ and $F_{w,2}$ are the two weighted fake factors that can be constructed using the first and second loose leptons in the CR, respectively. The small contribution from irreducible and 1-fake lepton background processes in the CR, $N_{\mathrm{irr,1\text{-}fake}}^{\mathrm{CR}}$, is subtracted from the corresponding number of events seen in data.

6.1 Systematic uncertainties

Several sources of systematic uncertainties are considered for the SM background estimates and signal yield predictions. The primary sources of systematic uncertainty, described below, are summarized in Table 4.

Experimental (% of total SM)		Theoretical (% of each process)	
e efficiency	3.9%	σ: $t\bar{t}Z$	12%
μ efficiency	1.9–2.8%	σ: $t\bar{t}W$	13%
Jet energy scale	3.0–3.4%	σ: ZZ,WZ	6%
Luminosity	2.9%	σ: VVV/tWZ	20%
MC statistics	2.7–2.5%	$A\epsilon$: ZZ	56–80%
CR statistics	4.5–6.4%	$A\epsilon$: $t\bar{t}Z$	9–12%
		$\sigma A\epsilon$: VH/VBF H	20%
		$\sigma A\epsilon$: ggF H/ $t\bar{t}$H	100%

Table 4: Principal experimental and theoretical systematic uncertainties for the SM background estimation in the signal regions. For theoretical uncertainties, σ indicates an uncertainty on the production cross-section, while $A\epsilon$ indicates an uncertainty on the product of acceptance and efficiency.

The systematic uncertainties affecting the simulation-based estimates include the theoretical cross-section uncertainties due to the choice of renormalisation and factorisation scales and PDFs, the acceptance uncertainty due to PDFs, the choice of MC generator, the uncertainty on the luminosity (following a methodology similar to that detailed in Ref. [53]), the uncertainty due to the jet energy scale, jet energy resolution, jet vertex tagger, lepton energy scale, lepton energy resolution and lepton identification efficiency, and the uncertainty on the $E_{\mathrm{T}}^{\mathrm{miss}}$ from energy deposits not associated with reconstructed objects. The systematic uncertainty associated with the simulation of pile-up is also taken into account.

The theoretical cross-section uncertainties for the irreducible and 1-fake lepton backgrounds used in this analysis are 12% for $t\bar{t}Z$, 13% for $t\bar{t}W$, 6% for ZZ and WZ, and 20% for the triboson samples, as summarized in Table 4. For the Higgs boson samples, an uncertainty of 20% is used for VH and vector-boson-fusion production, while an uncertainty of 100% is assigned to $t\bar{t}H$ and Higgs boson production via gluon fusion [54]. The uncertainties on $t\bar{t}H$ and Higgs boson production via gluon fusion are assumed to be large to account for uncertainties on the acceptance, while the inclusive cross-sections are known to better precision. Uncertainties arising from the choice of generator are determined by comparing the Powheg and Sherpa generators for ZZ, and the MadGraph and Sherpa generators for $t\bar{t}Z$. The choice of generator dominates the uncertainty on ZZ in the signal regions. The uncertainty on the ZZ and $t\bar{t}Z$ acceptance due to PDF and scale variations is also studied.

The uncertainty on the 2-fake lepton reducible background is dominated by the statistical uncertainty on the data events in the CR, and also includes the MC statistical uncertainty on the process fractions, the uncertainty on the fake lepton scale factors, and the statistical uncertainty from the fake factors measured in simulation.

Systematic uncertainties on the SUSY signal yields from experimental sources typically lie in the 5–20% range, while theoretical uncertainties on signal cross-sections are typically of the order of 10%.

6.2 Background modelling validation

The general modelling of both the irreducible and reducible backgrounds is tested in a low-m_{eff} validation region that is defined to be adjacent to, yet disjoint from, the signal regions, as shown in Table 3. The background model adopted in the VR is the same as in the SRs, with the irreducible and 1-fake lepton backgrounds obtained from MC simulation and the reducible background estimated from data using the fake factor method. The SM background in the VR is dominated by ZZ, $t\bar{t}$ and Z+jets.

Observed and expected event yields in the VR are shown in Table 5, where good agreement is seen within statistical and systematic uncertainties. The electron and muon p_{T} distributions in the VR are shown in Figure 2, while the m_{eff} distribution in the VR can be seen in the lower m_{eff} bins in Figure 3(a).

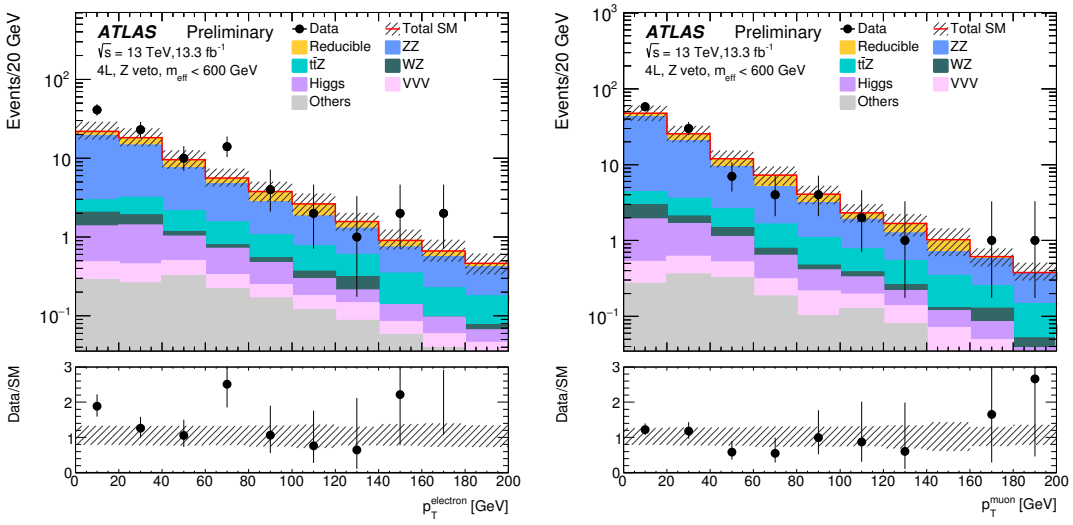

(a) (b)

Figure 2: For VR events, (a) the electron p_{T} and (b) the muon p_{T} distributions for data and the estimated SM backgrounds. The irreducible and 1-fake lepton backgrounds are estimated from MC simulation while the 2-fake lepton background is estimated from data. "Others" is the sum of the tWZ, $t\bar{t}WW$, $t\bar{t}t\bar{t}$, $tt\bar{t}$, and $t\bar{t}W$ backgrounds. Both the statistical and systematic uncertainties are included in the shaded band.

7 Results

The expected and observed yields in each signal region are reported in Table 5, together with the statistical and systematic uncertainties on the background predictions. Two events are observed in SRA in the 13.3 fb^{-1} dataset, while no events are observed in SRB; the observations are consistent with the SM expectation. The m_{eff} and $E_{\mathrm{T}}^{\mathrm{miss}}$ distributions for all events with four or more leptons that pass the Z boson veto are shown in Figure 3.

The HistFitter [55] software framework is used for the statistical interpretation of the results. In order to quantify the probability for the background-only hypothesis to fluctuate to the observed number of events or higher, a one-sided p_0-value is calculated using pseudoexperiments, where the profile likelihood ratio is used as a test statistic [56] to exclude the signal-plus-background hypothesis. A signal model can be excluded at 95% confidence level (CL) if the CL$_s$ [57] of the signal plus background hypothesis is <0.05. For each signal region, the expected and observed upper limits at 95% CL on the number of beyond-the-SM events (S_{exp}^{95} and S_{obs}^{95}) are calculated using the model-independent signal fit. The 95% CL upper limits on the signal cross-section times efficiency ($\langle\epsilon\sigma\rangle_{\mathrm{obs}}^{95}$) and the CL$_b$ value for the background-only hypothesis are also calculated for each signal region.

To set exclusion limits in the $LL\bar{E}12k$ models, the signal region with the best expected exclusion is used. All experimental uncertainties are treated as correlated between regions and processes, with the

Sample	VR	SRA	SRB
Irreducible			
ZZ	29 ± 5	0.6 ± 0.4	0.20 ± 0.19
$t\bar{t}Z$	2.05 ± 0.24	1.43 ± 0.23	0.47 ± 0.09
Higgs	1.7 ± 1.4	0.4 ± 0.4	0.11 ± 0.11
VVZ	0.72 ± 0.14	0.31 ± 0.06	0.123 ± 0.027
Others	0.28 ± 0.07	0.32 ± 0.04	0.181 ± 0.022
1-fake ℓ reducible	1.14 ± 0.07	0.168 ± 0.018	0.069 ± 0.014
2-fake ℓ reducible	16 ± 6	0.48 ± 0.24	0.11 ± 0.05
Σ SM	51 ± 6	3.6 ± 0.6	1.26 ± 0.26
Data	53	2	0
p_0	—	0.64	0.80
S^{95}_{obs}	—	4.3	3.0
S^{95}_{exp}	—	$5.4^{+1.6}_{-1.3}$	$3.8^{+1.3}_{-0.8}$
$\langle\epsilon\sigma\rangle^{95}_{\text{obs}}$ [fb]	—	0.32	0.22
CL_b	—	0.21	0.15

Table 5: Expected and observed yields for 13.3 fb^{-1} in the 4L validation and signal regions. "Others" is the sum of the tWZ, $t\bar{t}WW$, $t\bar{t}t\bar{t}$ and $tt\bar{t}$ backgrounds. Statistical and systematic uncertainties are included. Also shown are the model-independent limits calculated from the signal region observations: a one-sided p_0-value; the expected and observed upper limit at 95% CL on the number of beyond-the-SM events (S^{95}_{exp} and S^{95}_{obs}) for each signal region, calculated using pseudoexperiments and the CL_s prescription; the observed 95% CL upper limit on the signal cross-section times efficiency ($\langle\epsilon\sigma\rangle^{95}_{\text{obs}}$); and the CL_b value for the background-only hypothesis.

exception of the experimental uncertainties on data-driven backgrounds, which are correlated between regions only. Theoretical uncertainties on the irreducible background and signal are treated as correlated between regions, while statistical uncertainties from MC simulation and data in the CR are treated as uncorrelated between regions and processes. For the exclusion limits, the observed and expected 95% CL limits are calculated using the Asimov dataset for each SUSY model point, taking into account the theoretical and experimental uncertainties on the SM background and the experimental uncertainties on the signal. The impact of the theoretical uncertainties on the signal cross-section is shown for the observed mass limit; where quoted in the text, the mass limits refer to the observed limit without considering signal cross-section uncertainties.

Figure 4 shows the exclusion contour of the $LL\bar{E}12k$ model, where $\tilde{\chi}^{\pm}_1$ with masses up to 1.14 TeV are excluded for $m(\tilde{\chi}^0_1) > 500$ GeV. The sensitivity is reduced where the decay products are boosted for large mass splittings between the $\tilde{\chi}^{\pm}_1$ and the $\tilde{\chi}^0_1$, and $\tilde{\chi}^{\pm}_1$ masses up to 1.07 TeV are excluded. This extends the limits set in Ref. [16] by around 400 GeV.

8 Conclusion

Results are reported from a search for new physics in the final state with four or more leptons (electrons or muons), no Z boson candidates, and large effective mass. The analysis is based on 13.3 fb^{-1} of proton-proton collision data delivered by the LHC at $\sqrt{s} = 13$ TeV in 2015 and 2016. No significant excess of

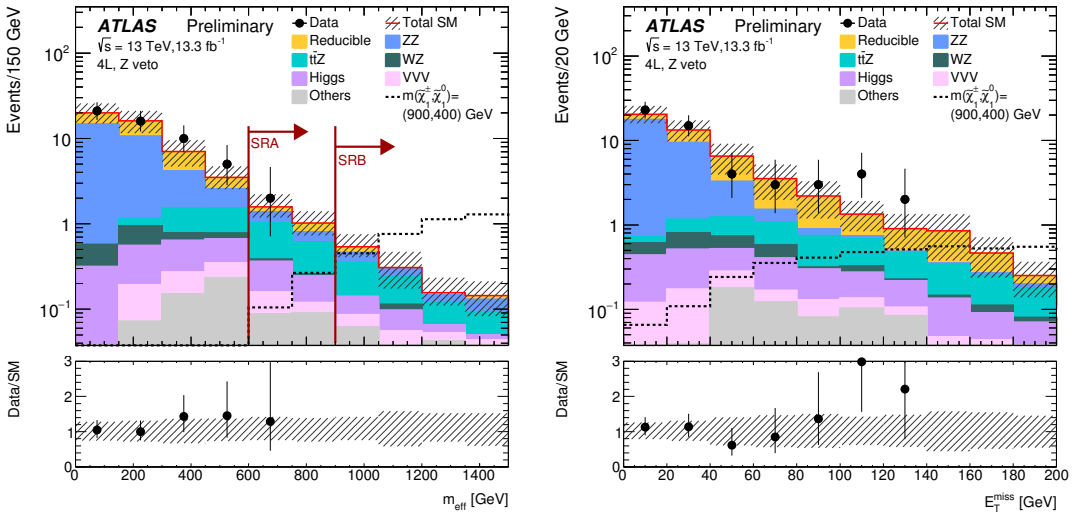

(a) (b)

Figure 3: For events with four or more leptons that pass the Z veto requirement, (a) the m_{eff} and (b) the $E_{\text{T}}^{\text{miss}}$ distributions for data, the estimated SM backgrounds, and an example SUSY scenario. The irreducible and 1-fake lepton backgrounds are estimated from MC simulation while the 2-fake lepton background is estimated from data. "Others" is the sum of the tWZ, $t\bar{t}WW$, $t\bar{t}t\bar{t}$, $tt\bar{t}$, and $t\bar{t}W$ backgrounds. Both the statistical and systematic uncertainties are included in the shaded band. The red arrows indicate the m_{eff} selections in the signal regions. The region with $m_{\text{eff}} < 600$ GeV is used to validate the SM background modelling.

events is found in data. The null result is interpreted in a simplified model of chargino pair production with indirect RPV decays, where chargino masses up to 1.14 TeV are excluded for large LSP masses.

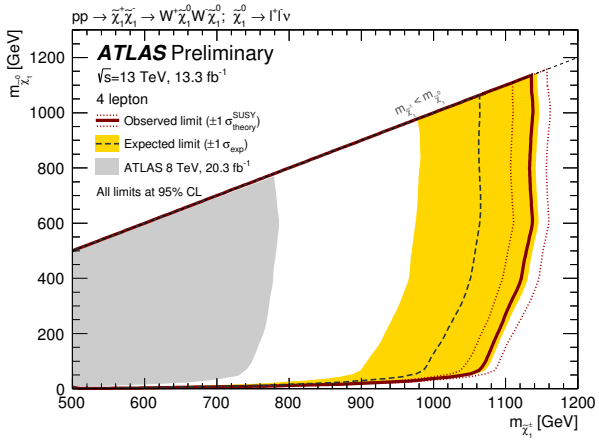

Figure 4: The 95% CL exclusion limits on chargino production with indirect RPV decays via λ_{12k}, where $k = 1, 2$. The limits are set using the signal region with the best expected exclusion. The 8 TeV limit from Ref. [16] is also shown.

Appendix

Cleaning Requirement	Efficiency
GRL Requirement	0.938
LAr Error Rejection	0.937
Trigger Requirement	0.834
Primary Vertex	0.834
Bad Jet Cleaning	0.831
Cosmic Muon Rejection	0.753
Bad Muon Rejection	0.753

Table 6: The selection efficiency of cleaning requirements, where the denominator is the number of data events with at least two leptons with $p_{\mathrm{T}} > 9$ GeV.

$m(\tilde{\chi}_1^{\pm}, \tilde{\chi}_1^0)$ [GeV]	1000, 800		1000, 400		1000, 10	
Initial	7.7	(4996)	7.7	(4996)	7.3	(26529)
Trigger	7.6	(4990)	7.7	(4993)	7.0	(25490)
Event cleaning	7.4	(4844)	7.5	(4860)	6.9	(24788)
$N_\ell \geq 1$	7.4	(4839)	7.5	(4852)	5.8	(20804)
$N_\ell \geq 2$	7.4	(4820)	7.5	(4829)	4.7	(17099)
$N_\ell \geq 3$	7.1	(4648)	7.1	(4557)	2.7	(9502)
$N_\ell \geq 4$	5.6	(3599)	5.4	(3472)	1.2	(4182)
Z veto	5.3	(3389)	4.8	(3093)	1.1	(3739)
$m_{\mathrm{eff}} > 600$ GeV	5.3	(3388)	4.8	(3087)	1.1	(3711)
$m_{\mathrm{eff}} > 900$ GeV	5.3	(3351)	4.7	(3008)	0.96	(3546)
$m(\tilde{\chi}_1^{\pm}, \tilde{\chi}_1^0)$ [GeV]	500, 490		500, 200		500, 10	
Initial	274	(4985)	271	(4988)	259	(9122)
Trigger	274	(4981)	271	(4979)	248	(8765)
Event cleaning	268	(4863)	264	(4829)	242	(8526)
$N_\ell \geq 1$	267	(4850)	261	(4785)	194	(6869)
$N_\ell \geq 2$	266	(4827)	258	(4738)	160	(5641)
$N_\ell \geq 3$	251	(4527)	233	(4272)	90	(3225)
$N_\ell \geq 4$	178	(3143)	162	(2968)	38	(1375)
Z veto	160	(2845)	109	(2012)	30	(1020)
$m_{\mathrm{eff}} > 600$ GeV	150	(2667)	97	(1808)	26	(901)
$m_{\mathrm{eff}} > 900$ GeV	89	(1514)	54	(952)	14	(484)

Table 7: Cutflows for different SUSY signals with $m(\tilde{\chi}_1^{\pm}) = 1000$ GeV or $m(\tilde{\chi}_1^{\pm}) = 500$ GeV. The table lists the expected yields for 13.3 fb^{-1} taken from MC directly. The numbers in brackets represent the actual number of MC events that passed the specific cut. The event cleaning includes the requirement of a reconstructed vertex, the veto of misreconstructed jets and muon, as well as the veto of the cosmic muons.

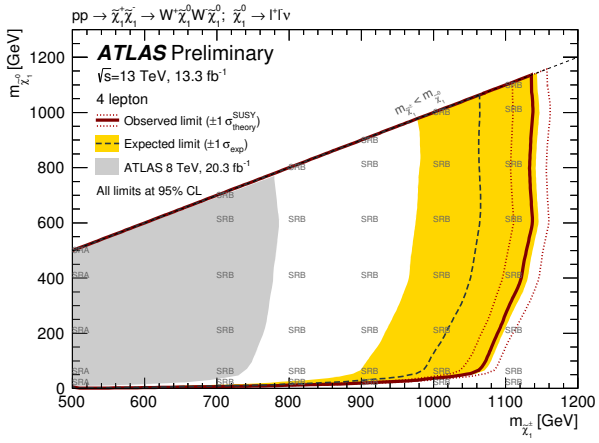

Figure 5: The signal region with the best expected exclusion power at each point in the signal grid.

References

[1] Yu. A. Golfand and E. P. Likhtman,
Extension of the Algebra of Poincare Group Generators and Violation of p Invariance,
JETP Lett. **13** (1971) 323, [Pisma Zh. Eksp. Teor. Fiz.13,452(1971)].

[2] D. V. Volkov and V. P. Akulov, *Is the Neutrino a Goldstone Particle?*, Phys. Lett. B **46** (1973) 109.

[3] J. Wess and B. Zumino, *Supergauge Transformations in Four-Dimensions*,
Nucl. Phys. B **70** (1974) 39.

[4] J. Wess and B. Zumino, *Supergauge Invariant Extension of Quantum Electrodynamics*,
Nucl. Phys. B **78** (1974) 1.

[5] S. Ferrara and B. Zumino, *Supergauge Invariant Yang-Mills Theories*,
Nucl. Phys. B **79** (1974) 413.

[6] A. Salam and J. A. Strathdee, *Supersymmetry and Nonabelian Gauges*,
Phys. Lett. B **51** (1974) 353.

[7] N. Sakai, *Naturalness in Supersymmetric Guts*, Z. Phys. C **11** (1981) 153.

[8] S. Dimopoulos, S. Raby and F. Wilczek, *Supersymmetry and the Scale of Unification*,
Phys. Rev. D **24** (1981) 1681.

[9] L. E. Ibanez and G. G. Ross, *Low-Energy Predictions in Supersymmetric Grand Unified Theories*,
Phys. Lett. B **105** (1981) 439.

[10] S. Dimopoulos and H. Georgi, *Softly Broken Supersymmetry and SU(5)*,
Nucl. Phys. B **193** (1981) 150.

[11] S. Weinberg, *Supersymmetry at Ordinary Energies. 1. Masses and Conservation Laws*,
Phys. Rev. D **26** (1982) 287.

[12] N. Sakai and T. Yanagida, *Proton Decay in a Class of Supersymmetric Grand Unified Models*,
Nucl. Phys. B **197** (1982) 533.

[13] S. Ahmed et al.,
Constraints on nucleon decay via 'invisible' modes from the Sudbury Neutrino Observatory,
Phys. Rev. Lett. **92** (2004) 102004, arXiv: hep-ex/0310030.

[14] G. R. Farrar and P. Fayet, *Phenomenology of the Production, Decay, and Detection of New Hadronic States Associated with Supersymmetry*, Phys. Lett. B **76** (1978) 575.

[15] ATLAS Collaboration, *Search for R-parity-violating supersymmetry in events with four or more leptons in $\sqrt{s}$ = 7 TeV pp collisions with the ATLAS detector*, JHEP **12** (2012) 124, arXiv: 1210.4457 [hep-ex].

[16] ATLAS Collaboration, *Search for supersymmetry in events with four or more leptons in $\sqrt{s}$ = 8 TeV pp collisions with the ATLAS detector*, Phys. Rev. D **90** (2014) 052001, arXiv: 1405.5086 [hep-ex].

[17] V. Abazov et al., *Search for supersymmetry via associated production of charginos and neutralinos in final states with three leptons*, Phys. Rev. Lett. **95** (2005) 151805, arXiv: hep-ex/0504032.

[18] V. Abazov et al., *Search for associated production of charginos and neutralinos in the trilepton final state using 2.3 fb^{-1} of data*, Phys. Lett. B **680** (2009) 34, arXiv: 0901.0646 [hep-ex].

[19] V. Abazov et al., *Search for R-parity violating supersymmetry via the LL anti-E couplings λ_{121}, λ_{122} or λ_{133} in $p\bar{p}$ collisions at $\sqrt{s}$ = 1.96-TeV*, Phys. Lett. B **638** (2006) 441, arXiv: hep-ex/0605005.

[20] T. Aaltonen et al., *Search for chargino-neutralino production in $p\bar{p}$ collisions at $\sqrt{s}$ = 1.96-TeV*, Phys. Rev. Lett. **99** (2007) 191806, arXiv: 0707.2362 [hep-ex].

[21] T. Aaltonen et al., *Search for Supersymmetry in $p\bar{p}$ Collisions at $\sqrt{s}$ = 1.96-TeV Using the Trilepton Signature of Chargino-Neutralino Production*, Phys. Rev. Lett. **101** (2008) 251801, arXiv: 0808.2446 [hep-ex].

[22] A. Abulencia et al., *Search for anomalous production of multi-lepton events in $p\bar{p}$ collisions at $\sqrt{s}$ = 1.96-TeV*, Phys. Rev. Lett. **98** (2007) 131804, arXiv: 0706.4448 [hep-ex].

[23] ATLAS Collaboration, *SUSY Searches at ATLAS in Multilepton Final States with Jets and Missing Transverse Energy*, ATLAS-CONF-2011-039, 2011, URL: http://cdsweb.cern.ch/record/1338568.

[24] ATLAS Collaboration, *Search for supersymmetry in events with three leptons and missing transverse momentum in $\sqrt{s}$ = 7 TeV pp collisions with the ATLAS detector*, Phys. Rev. Lett. **108** (2012) 261804, arXiv: 1204.5638 [hep-ex].

[25] ATLAS Collaboration, *Search for direct production of charginos and neutralinos in events with three leptons and missing transverse momentum in $\sqrt{s}$ = 8 TeV pp collisions with the ATLAS detector*, JHEP **04** (2014) 169, arXiv: 1402.7029 [hep-ex].

[26] CMS Collaboration, *Search for Physics Beyond the Standard Model Using Multilepton Signatures in pp Collisions at $\sqrt{s}$ = 7 TeV*, Phys. Lett. B **704** (2011) 411, arXiv: 1106.0933 [hep-ex].

[27] CMS Collaboration, *Search for anomalous production of multilepton events in pp collisions at $\sqrt{s}$ = 7 TeV*, JHEP **06** (2012) 169, arXiv: 1204.5341 [hep-ex].

[28] CMS Collaboration, *Search for electroweak production of charginos and neutralinos using leptonic final states in pp collisions at $\sqrt{s}$ = 7 TeV*, JHEP **11** (2012) 147, arXiv: 1209.6620 [hep-ex].

[29] CMS Collaboration, *Search for top squarks in R-parity-violating supersymmetry using three or more leptons and b-tagged jets*, Phys. Rev. Lett. **111** (2013) 221801, arXiv: 1306.6643 [hep-ex].

[30] CMS Collaboration, *Search for anomalous production of events with three or more leptons in pp collisions at* $\sqrt{s} = 8$ *TeV*, Phys. Rev. D **90** (2014) 032006, arXiv: 1404.5801 [hep-ex].

[31] ATLAS Collaboration, *Constraints on promptly decaying supersymmetric particles with lepton-number- and R-parity-violating interactions using Run-1 ATLAS data*, ATLAS-CONF-2015-018, 2015, URL: http://cdsweb.cern.ch/record/2017303.

[32] B. Fuks, M. Klasen, D. R. Lamprea and M. Rothering, *Gaugino production in proton-proton collisions at a center-of-mass energy of 8 TeV*, JHEP **10** (2012) 081, arXiv: 1207.2159 [hep-ph].

[33] B. Fuks, M. Klasen, D. R. Lamprea and M. Rothering, *Precision predictions for electroweak superpartner production at hadron colliders with Resummino*, Eur. Phys. J. C **73** (2013) 2480, arXiv: 1304.0790 [hep-ph].

[34] ATLAS Collaboration, *The ATLAS Experiment at the CERN Large Hadron Collider*, JINST **3** (2008) S08003.

[35] ATLAS Collaboration, 'ATLAS Insertable B-Layer Technical Design Report', CERN-LHCC-2010-013, URL: http://cds.cern.ch/record/1291633.

[36] ATLAS Collaboration, *2015 start-up trigger menu and initial performance assessment of the ATLAS trigger using Run-2 data*, ATL-DAQ-PUB-2016-001, 2016, URL: http://cds.cern.ch/record/2136007.

[37] S. Agostinelli et al., *GEANT4: A simulation toolkit*, Nucl. Instrum. Meth. A **506** (2003) 250.

[38] ATLAS Collaboration, *The ATLAS Simulation Infrastructure*, Eur. Phys. J. C **70** (2010) 823, arXiv: 1005.4568 [hep-ex].

[39] J. Alwall et al., *The automated computation of tree-level and next-to-leading order differential cross sections, and their matching to parton shower simulations*, JHEP **07** (2014) 079, arXiv: 1405.0301 [hep-ph].

[40] T. Sjöstrand et al., *An Introduction to PYTHIA 8.2*, Comput. Phys. Commun. **191** (2015) 159, arXiv: 1410.3012 [hep-ph].

[41] T. Gleisberg, S. Höche, F. Krauss, M. Schönherr, S. Schumann et al., *Event generation with SHERPA 1.1*, JHEP **02** (2009) 007, arXiv: 0811.4622 [hep-ph].

[42] S. Frixione and B. R. Webber, *Matching NLO QCD computations and parton shower simulations*, JHEP **06** (2002) 029, arXiv: hep-ph/0204244.

[43] S. Alioli, P. Nason, C. Oleari and E. Re, *A general framework for implementing NLO calculations in shower Monte Carlo programs: the POWHEG BOX*, JHEP **06** (2010) 043, arXiv: 1002.2581 [hep-ph].

[44] T. Sjöstrand, S. Mrenna and P. Z. Skands, *PYTHIA 6.4 Physics and Manual*, JHEP **05** (2006) 026, arXiv: hep-ph/0603175.

[45] J. Alwall, M. Herquet, F. Maltoni, O. Mattelaer and T. Stelzer, *MadGraph 5 : Going Beyond*, JHEP **06** (2011) 128, arXiv: 1106.0522 [hep-ph].

[46] ATLAS Collaboration,
Electron identification measurements in ATLAS using $\sqrt{s}$ = 13 TeV data with 50 ns bunch spacing,
ATL-PHYS-PUB-2015-041, 2015, URL: http://cdsweb.cern.ch/record/2048202.

[47] ATLAS Collaboration, *Muon reconstruction performance of the ATLAS detector in proton–proton collision data at $\sqrt{s}$ =13 TeV*, Eur. Phys. J. C **76** (2016) 292, arXiv: 1603.05598 [hep-ex].

[48] M. Cacciari, G. P. Salam and G. Soyez, *The Anti-k_t jet clustering algorithm*, JHEP **04** (2008) 063, arXiv: 0802.1189 [hep-ph].

[49] ATLAS Collaboration, *Jet Calibration and Systematic Uncertainties for Jets Reconstructed in the ATLAS Detector at $\sqrt{s}$ = 13 TeV*, ATL-PHYS-PUB-2015-015, 2015,
URL: https://cds.cern.ch/record/2037613.

[50] ATLAS Collaboration, *Tagging and suppression of pileup jets with the ATLAS detector*,
ATLAS-CONF-2014-018, 2014, URL: http://cdsweb.cern.ch/record/1700870.

[51] ATLAS Collaboration, *Jet Calibration and Systematic Uncertainties for Jets Reconstructed in the ATLAS Detector at $\sqrt{s}$ =13 TeV*, ATL-PHYS-PUB-2015-015, 2015,
URL: http://cds.cern.ch/record/2037613.

[52] ATLAS Collaboration, *Performance of missing transverse momentum reconstruction for the ATLAS detector in the first proton-proton collisions at $\sqrt{s}$ =13 TeV*, ATL-PHYS-PUB-2015-027,
2015, URL: http://cds.cern.ch/record/2037904.

[53] ATLAS Collaboration, *Improved luminosity determination in pp collisions at $\sqrt{s}$ = 7 TeV using the ATLAS detector at the LHC*, Eur. Phys. J. C **73** (2013) 2518, arXiv: 1302.4393 [hep-ex].

[54] S. Dittmaier et al., *Handbook of LHC Higgs Cross Sections: 2. Differential Distributions*, (2012),
arXiv: 1201.3084 [hep-ph].

[55] M. Baak et al., *HistFitter software framework for statistical data analysis*,
Eur. Phys. J. C **75** (2015) 153, arXiv: 1410.1280 [hep-ex].

[56] G. Cowan, K. Cranmer, E. Gross and O. Vitells,
Asymptotic formulae for likelihood-based tests of new physics,
Eur. Phys. J. C **71** (2011) 1554, [Erratum: Eur. Phys. J.C73,2501(2013)],
arXiv: 1007.1727 [physics.data-an].

[57] A. L. Read, *Presentation of search results: The CL(s) technique*, J. Phys. G **28** (2002) 2693.